Submitted to *Physical Review B*

Polarization dependence of resonant Raman scattering from vertically aligned SWNT films

Yoichi Murakami, Shohei Chiashi, Erik Einarsson and Shigeo Maruyama*

Department of Mechanical Engineering, The University of Tokyo

7-3-1 Hongo, Bunkyo-ku, Tokyo 113-8656, Japan

Abstract

We present experimental evidence of drastic changes in low-frequency Raman scattering spectra depending on the polarization of the incident laser with respect to the single-walled carbon nanotube (SWNT) axis. Employing recently developed vertically aligned SWNT films, which have a high density (1.0×10^{17} m^{-2}) and a thickness of 5 μm, enabled us to obtain sufficient Raman scattering intensity from the film cross-section where bundles of SWNTs are aligned along the same direction, in addition to from the top surface of the film. The measured peaks of the radial breathing mode (RBM) by 1.96, 2.41, and 2.54 eV incident lasers are clearly distinguished into 2 groups. One group of peaks is dominant for perpendicular polarization while other group of peaks is dominant in the case of light polarized parallel to the SWNT axis. The selective vanishing of the perpendicular peaks by

adsorption of molecules to the SWNTs along with the resultant change in optical absorption spectrum evidences that the parallel and perpendicular peaks originate from $\Delta\mu = 0$ and $\Delta\mu = \pm 1$ excitations of electrons, respectively. The grouping behavior of RBM peaks also causes the drastic spectral variation caused by a change in incident laser power. The unambiguous classification of each RBM peak's nature presented in this study will allow sounder characterization of SWNTs by the resonant Raman scattering analysis.

PACS #: 78.30.Na, 78.67.Ch

*Corresponding Author. Tel & Fax: +81-3-5800-6983.

E-mail address: maruyama@photon.t.u-tokyo.ac.jp (S. Maruyama).

I. INTRODUCTION

Resonant Raman scattering (RRS) spectroscopy has been an important tool to obtain structural information including quality and diameter, as well as distinguishing between metallic and semiconducting single-walled carbon nanotubes (SWNTs).[1-3] In the radial breathing mode (RBM) that appears in lower frequency region, the resonant nature of

electronic transitions between Van Hove singularities in the valence and conduction bands has been utilized to experimentally probe for chiral distribution of SWNTs.[4-7] It was demonstrated experimentally by Jorio and co-workers[8] that, from their RRS measurements on G-band modes of isolated SWNTs, the possibility of $\Delta\mu = \pm 1$ transitions should be taken into account in addition to the usual $\Delta\mu = 0$ transition (μ denotes the cutting-line index[1,8]). Understanding the significance of the $\Delta\mu = \pm 1$ transition is important because it crucially affects the interpretation of RBM spectra needed for the assignment of chirality as well as the distinction between metallic and semiconducting SWNTs based on the Kataura plot.[9] Several theoretical works[10-12] indicated that the $\Delta\mu = \pm 1$ transition is induced by absorption of light polarized across the SWNT axis, and hence polarized Raman analysis should be effective to study this subject.

So far several studies employing polarized RRS on SWNTs, either bundled or isolated, have been reported.[8,13-17] While some of them focused solely on the G-band's intensity and structure by changing the polarization direction,[8,13,16] a small number of papers investigated the dependence of the RBM by the change of polarization. Hwang et al.[14] and Duesberg et al.[15] performed polarized RRS experiments on nearly isolated SWNTs on a glass plate and presumably bundled SWNTs aligned in a melt-spun PMMA fiber, respectively, and showed

that the scattering intensities of both RBM and G peaks are maximized when the polarization of the light is parallel to the SWNT axis and are suppressed when perpendicular. In both reports the change of only one isolated RBM peak was presented at a fixed laser wavelength. Grüneis et al.[17] recently reported, from their Raman measurement on randomly-oriented SWNT bundles, unexpected RBM peaks between E^{S}_{22} and E^{M}_{11} (subscript number denotes serial number of Van Hove singularities) that apparently deviated from their tight-binding-based Kataura plot as well as from the data based on photo-luminescence.[18] They reported that the unexpected RBM peaks were an observation of $\Delta\mu = \pm 1$ excitations caused by the absorption by SWNTs of perpendicularly polarized light[17], because the dipole selection rules give different absorption energies for light with parallel and perpendicular polarization.[10-12] They discussed that, in contrast to isolated SWNTs, bundled SWNTs could absorb the cross-polarized light due to an imperfection of the "depolarization effect" that was predicted by Ajiki and Ando.[10] Since all the RBM peaks measured from their randomly aligned and bundled SWNTs were plotted[17] the peaks had not been unambiguously classified especially in the higher energy region above E^{M}_{11} on the Kataura plot, where the E_{ii} plots start to broaden and overlap each other.[9]

Recently, our group developed a method to synthesize vertically aligned SWNT films directly on the surface of quartz substrates[19], using the alcohol chemical vapor deposition (ACCVD) method[20,21]. Since this SWNT film has a macroscopic thickness (approximately 5 μm) and is uniform over the substrate (25 × 25 mm^2),[19,22] it is ideal for optical measurements including Raman scattering analysis. In this report, we demonstrate that the spectral shape of the RBM from this aligned SWNT film exhibits a remarkable dependence on the relationship between the light polarization vector (***e***) and the SWNT axis direction (***l***). The obtained spectra was analyzed quantitatively and we conclude that each specified peak falls clearly into one of two groups, where the peaks in one group dominate for the case of $\boldsymbol{e} \perp \boldsymbol{l}$ and the others dominate for $\boldsymbol{e} \parallel \boldsymbol{l}$. The grouping of RBM peaks is also observed by the difference in behavior toward an adsorption of molecules and a change in the incident laser power. These results evidence the $\boldsymbol{e} \parallel \boldsymbol{l}$ and $\boldsymbol{e} \perp \boldsymbol{l}$ peaks are $\Delta\mu = 0$ and $\Delta\mu = \pm 1$ resonance, respectively. From the experimental investigations performed in this report, we unambiguously distinguish both types of RBM peaks in a higher energy range (1.96 - 2.54 eV) that are often used in RRS analysis of SWNTs, over wide range of tube diameter (0.8 - 1.8 nm).

II. EXPERIMENTAL SETUP

When performing Raman scattering measurements we used a micro-Raman setup (Seki Technotron, STR-250) composed of an optical microscope (Olympus, BX51), a spectrometer (Chromex, 501is) and a CCD (Andor, DV401-FI). Laser wavelengths of 488 (2.54), 514.5 (2.41) and 633 nm (1.96 eV) were used. The measurements were done in back-scattering configuration with an incident laser power of 0.2 - 0.5 mW with a spot size $\geq$ 5 μm at the sample surface and a 50X objective lens, unless otherwise stated. The energy density used in this study ($\leq$ 2.5×10^3 W/cm^2) is chosen to be sufficiently low compared with that typically used in micro Raman measurement on SWNTs (e.g. 1×10^6 W/cm^{-2} in Ref. 23), in order to avoid any unexpected effects on Raman spectra caused by laser heating.[24,25] Specifically, we monitored the location of the G^+ band (at approximately 1593 cm^{-1} at room temperature[25,26]) to make sure it did not descend below 1592 cm^{-1} (or above 100°C[25,26]) during the measurements. The laser light incident on the sample was linearly polarized by a polarizer put in the path of the laser light. Scattered light was collected back into the microscope, passing a half mirror and then a depolarizer before entering the spectrometer. In some experiments (in Fig. 4) we placed a polarizer just before the depolarizer in order to check the spectral dependence on the polarization of scattered

light. Before every series of measurements the spectrometer was calibrated with sulfur (153.8, 219.1 and 473.2 cm^{-1}) and naphthalene (1382.2 and 1576.6 cm^{-1}) characteristic peaks.

III. RESULTS

A. Raman spectrum dependence on laser polarization

Figure 1 shows an FE-SEM micrograph of the vertically aligned SWNTs taken from the side at the fractured edge of the substrate. The film thickness is around 5 μm and aligned bundles of SWNTs are visible, which typically have diameter of approximately 15 nm. The overall density of SWNTs has been estimated to be $\approx 1.0 \times 10^{17}$ m^{-2}.[19] From TEM observations, it has been confirmed that no MWNTs are present, and almost all SWNTs are clean i.e. free of amorphous carbon.[27] According to TEM measurements this specimen has a diameter distribution ranging from $d = 0.8 \sim 3.0$ nm, with an average diameter $d_{av} \approx 1.9$ nm and a standard deviation $\sigma = 0.4 \sim 0.5$ nm.[27] This distribution is exceptionally broad compared to typical arc-discharge and laser-furnace (within ± 0.2 nm),[9] HiPco SWNTs (d_{av} = 0.98 nm, σ = 0.2 nm),[28] and ACCVD SWNTs grown on zeolite powder at 650°C,[29] and therefore it is suitable for probing a wide range of chiralities at the same time.

In the following, we use 4 different configurations of the laser propagation direction (***k***), the laser polarization direction (***e***), and the SWNT axis direction (***l***) as schematized in Fig. 2. The "From top" configuration is $\boldsymbol{k} \,//\, \boldsymbol{l}$ and $\boldsymbol{e} \perp \boldsymbol{l}$, where laser is incident perpendicular to the substrate (or the SWNT film). In the "perpendicular" and "parallel" configurations, the relationships are $\{\boldsymbol{k} \perp \boldsymbol{l}$ and $\boldsymbol{e} \perp \boldsymbol{l}\}$ and $\{\boldsymbol{k} \perp \boldsymbol{l}$ and $\boldsymbol{e} \,//\, \boldsymbol{l}\}$, respectively, and in the "45°" configuration the angle between ***e*** and ***l*** is 45° while maintaining $\boldsymbol{k} \perp \boldsymbol{l}$. In the latter 3 cases, the quartz substrate supporting the SWNT film was broken and stood on its edge using adhesive tape in order to measure on the cross-section of the film.

Figure 3 shows RBM spectra taken in (i) from top, (ii) perpendicular, (iii) 45° and (iv) parallel configurations for 488, 514.5, and 633 nm laser wavelengths. On the top of each panel, corresponding diameter scale calculated by the formula 'd (nm) = 248 / ν (cm^{-1})' is presented.[5] Although several formulae have been proposed, such as 'd (nm) = 234 / ν (cm^{-1})' from *ab initio* calculations[30,31] and 'd (nm) = (223.5)/ (ν - 12.5) (cm^{-1})' from the measurement on micelle-dispersed HiPco SWNTs[32], the differences in 'd' calculated from these formula are within 6 % for the considered range. Establishment of more correct formula for describing the relation between the Raman shift and the diameter has been desired. In the 488 nm case, the high frequency spectra including D and G bands are also

shown. All the RBM peaks were normalized by the height of G^+ band at 1593 cm^{-1}. The G^+ band was used for the normalization of the spectra assuming it represents resonance, although it is known that the G^+ peak as well as G^- peak are composed of A_1 and E_1 modes located very close (~ 2 cm^{-1}) to each other.[8] At each wavelength, the spectra of cases (i) and (ii) (where $\boldsymbol{e} \perp \boldsymbol{l}$) show the same shape while that of case (iv) (where $\boldsymbol{e} \,//\, \boldsymbol{l}$) exhibits a remarkably different spectral shape. The spectra in case (iii) lie in the intermediate between (i) and (iv). It is obvious that some peaks are observed with certain intensities only in the $\boldsymbol{e} \perp \boldsymbol{l}$ case and diminish in the $\boldsymbol{e} \,//\, \boldsymbol{l}$ configuration, while the other group behaves oppositely. This is especially remarkable for the 488 and 514.5nm cases.

We decomposed these spectra into Lorentzian curves, keeping the full-width half-maximum (FWHM) of the peaks within each spectra the same. For 633 nm we employed the location of E^S_{22} and E^M_{11} peaks in 180 - 300 cm^{-1} presented by Strano[33] from the photoluminescence experiments: For the range below 180 cm^{-1}, due to the absence of data, we set peak locations so that the sum of the Lorentzian peaks consistently fits all cases. As for 488 and 514.5 nm, since no consistent set of data has been reported in the higher energy region for E^S_{33} and E^S_{44}, we performed decomposition using the least number of

peaks necessary for consistent fitting. We allowed ±1 cm^{-1} freedom to each peak's location based on the resolution of our Raman measurement system.

A slight downshift of G^+ peak from 1593 to 1592 cm^{-1} is seen in the "parallel" configuration due primarily to heating of the SWNTs by the laser, which is more significant when $\boldsymbol{e}$ // $\boldsymbol{l}$ because light absorption is much enhanced.[27] It is noted that even when the incident laser intensity is further lowered (laser power of 0.1 mW with a spot size of ≈ 7 μm, corresponding to ≈ 250 W/cm^{-2}), the measured spectral shapes for (i) ~ (iv) are essentially the same as those shown in Fig. 3, with only a lowered signal-to-noise (S/N) ratio in these cases. Therefore, the spectral changes depending on the measurement condition in Fig. 3 are not those induced by the laser heating.

Figure 4 shows RBM spectra measured by polarized 488 nm light. To represent the polarization of both incident and scattered light we employ the "X-Y" description often used in polarized Raman studies.[13,15,16] A polarizer was inserted in the scattering light path, as stated above, except the "-All" cases. In Fig. 4(a) "V" and "H" denote polarization perpendicular and parallel to the SWNT axis, respectively. Therefore, it is noted that "V (vertical)" and "H (horizontal)" used here are relative to the SWNT axis. The intensity ratio of {V-V : V-H : H-H : H-V ≈ 40 : 15 : 100 : 15} at the G^+ band indicates the cross-term

"V-H" and "H-V" (either intrinsically or due to disorder in the SWNT alignment) is so weak that the spectra of "V-all" and "H-all" are essentially the same as "V-V" and "H-H". Figure 4(b) shows the same measurement but the light is incident perpendicularly to the substrate in the "from top" configuration, which confirms that in the case of $\boldsymbol{k} \parallel \boldsymbol{l}$ the scattering spectra are independent of "X-Y" relation, as expected.

Figures 5(a) and (b) show the change of the height of selected Lorentzian peaks shown in Fig. 3 divided by the G^+ intensity among the "from top" - "45°" - "parallel" conditions for 488 and 514.5 nm. The ordinate for each peak is normalized by the value in the case of "from top", to show the grouping behavior of the RBM peaks toward the polarization. The collective peak at 185 cm^{-1} for 514.5 nm is decomposed into two adjacent peaks of at 183 and 188 cm^{-1}. Although some ambiguity remains in the quantitative decomposition, we recognize the 188 cm^{-1} peak to be $\boldsymbol{e} \,//\, \boldsymbol{l}$ peak based on Fig. 3. The peaks apparently associated with the $\boldsymbol{e} \,//\, \boldsymbol{l}$ configuration for 488 nm and 514.5 nm are {160 and 203 cm^{-1}} and {152 and 188 cm^{-1}}, respectively. As for the 633 nm case, since nearly 20 E^S_{22} and E^M_{11} peaks are plotted by Strano[33] within 1.96 ± 0.1 eV in the 180 - 300 cm^{-1} range, it was difficult to unambiguously classify each peak into the either of the two groups according to

our decomposition method: however, at least the peaks observed at 148, 164, and 217 cm^{-1} should be the $\boldsymbol{e} \,//\, \boldsymbol{l}$ peaks as identified in Fig. 3.

B. RBM peak behavior by molecular adsorption

It is noteworthy that within the "from top" measurement we can suppress the $\boldsymbol{e} \perp \boldsymbol{l}$ peaks by adsorbing some kind of molecules onto the SWNTs. Our CVD chamber used for SWNT growth is evacuated by an oil-free pump (ULVAC, DVS-321).[19] However, if the specimen is put in a chamber evacuated by ordinary oil-pumps (e.g. ULVAC GVD-050, ALCATEL 2015I) in our laboratory the spectrum shows the same change as was observed from (i) to (iv) in Fig. 3. Figure 6 shows this change measured in the "from top" condition with 488 nm light. The spectrum of an as-synthesized sample [Fig. 6(a)] is changed into that shown in Fig. 6(b) after evacuation for 1 h by the oil-pump. This spectral change is reversible, as the spectrum of a different molecule-adsorbed sample [Fig. 6(c)] prepared by the same method is readily recovered by heating it at 200°C for 1 h in the CVD chamber evacuated by the oil-free pump [Fig. 6(d)]. We have determined neither the adsorption molecule species nor microscopic adsorption details, but because of its relatively prompt recovery at low temperature (200°C), this easily reproduced result at least implies that this is a

physisorption of some oil-derived molecules diffused from the oil pumps. Slight blue-shift of the RBM frequency (~ 3 cm^{-1}) observed in Figs. 6(b) and (c), which is thought to be caused due to hardening of radial breathing motion of SWNTs by adhered molecules, agrees with the current discussion. The right panel of Fig. 6 shows higher frequency region of the left panel and no essential change between tangential modes of Figs. 6(a) and (b) is recognized. However, since the intensity of BWF peak[34] is originally weak in the case of before adsorption [Fig. 6(a)], we cannot perfectly negate the possibility of chemisorption by judging from the diminishing of BWF as observed by Strano et al.[35]. Furthermore, we have confirmed that a mere wetting of as-synthesized random SWNT ropes grown on catalyst-supporting zeolite powder by methanol decreases the peak at 180 cm^{-1} as measured by 488 nm light (results not shown), just as observed in Fig. 6. Therefore, it is certain that adsorption of some molecule (presumably organic) diminishes the RBM peaks that were preferentially observed for $\boldsymbol{e} \perp \boldsymbol{l}$, while peaks observed to dominate in the $\boldsymbol{e} \,//\, \boldsymbol{l}$ configuration are almost unaffected.

A series of experiments were performed in order to explain above experimental result. First, we let the vertically aligned SWNT film on a quartz substrate [whose Raman spectra shown in Fig. 7(a)] be adsorbed by the molecules and measured its optical absorption

spectrum [Fig. 7(b)]. Then the identical specimen was returned to it's original state by the method stated above and the optical absorption spectrum was measured again [Fig. 7(c)]. The effect of adsorption (or doping) on the optical absorption is more significant in the low energy region, closer to Fermi level (E_F), as was reported in Ref. 36. The reason of why only one group of RBM peak survives in the course of adsorption is understandable as follows. The peaks we observe in the $\boldsymbol{e} \,//\, \boldsymbol{l}$ configuration (corresponding to E^S_{33} and E^S_{44} peaks with energies of 2.41 and 2.54 eV) survive because, due to their depth below (i.e. approx. 1.21 and 1.27 eV) E_F, they are hardly doped. On the other hand, the peaks observed in the $\boldsymbol{e} \perp \boldsymbol{l}$ configuration diminish when doped because they were affected by the change of the electronic density close to E_F. This provides evidence that the $\boldsymbol{e} \perp \boldsymbol{l}$ peaks obtained so far have their origin in $\Delta\mu = \pm 1$ resonance that has been theoretically predicted,[10-12] some of which were found by Grüneis et al. in the lower energy region between E^S_{22} and E^M_{11} from a measurement of randomly oriented SWNT ropes.[17] The assignment of the $\boldsymbol{e} \perp \boldsymbol{l}$ peaks observed in this report to a specific energy band will be attempted later. A detailed investigation on the optical absorption spectrum of current SWNT film is shown in Ref. 27.

C. Raman spectrum dependence on laser intensity

Because of this essential difference in the character of RBM peaks, we can observe such grouping behavior under many experimental situations. Most notable is the dependence of the RBM spectral shape on the input laser power. Figure 8(a) shows the scattering from an as-synthesized specimen in the "from top" configuration with a 488 nm laser by varying its intensity from 0.75 to 2.42 mW. Figure 8(b) plots the height of each Lorentzian-decomposed peak normalized by that at 0.75 mW (ordinate) against the input laser power (absissa). While the intensities of the 160 and 203 cm^{-1} peaks corresponding to the $\Delta\mu = 0$ transition increase linearly with the laser power, the peaks corresponding to $\Delta\mu = \pm 1$ seem insensitive to the laser power, as if they were photo-saturated. Although the mechanism of this insensitiveness has yet to be determined, at least it can be said that the dual-nature of the RBM peak is responsible for the change of the RBM spectrum with the input power of the laser.

In Figure 8(a) some peaks were red-shifted due to the heating by the laser. Figure 8(c) plots the relative shift of each RBM peak against that of the G^+ band, both from the case of 0.75 mW. Obviously, while the $\boldsymbol{e} \parallel \boldsymbol{l}$ peaks shows a linear red shift of frequency as the temperature rises, the $\boldsymbol{e} \perp \boldsymbol{l}$ peaks are almost un-shifted. This is reasonably considered to

derive from the difference in the heating of tubes in the $\boldsymbol{e}$ // $\boldsymbol{l}$ and $\boldsymbol{e} \perp \boldsymbol{l}$ cases, because the light absorption of the former is several factors higher than the latter.[27]

Finally, in Figure 9, several unambiguous $\boldsymbol{e}$ // $\boldsymbol{l}$ (i.e. $\Delta\mu = 0$) peaks were marked with a circle and $\boldsymbol{e} \perp \boldsymbol{l}$ (i.e. $\Delta\mu = \pm 1$) peaks with a cross on a Kataura plot calculated using the tight-binding (solid symbols) and GW-methods[37] (open symbols). The tight binding DOS was calculated with $\gamma_0 = 2.9$ eV, $a_{c\text{-}c} = 0.144$ nm, and $s = 0.129$.[38] It is noted that these Kataura plots are different (especially for semiconducting SWNTs) from the plot based on fluorescence measurements;[18,33] however, it is still quantitatively effective to discuss the transition energies of metallic as well as semiconducting SWNTs for the higher energy (E^S_{33} and E^S_{44}) region where fluorescence measurements provide quite limited availability.

The upper row of Fig. 9 represents the plots for the $\Delta\mu = 0$ transition, while the lower row for the $\Delta\mu = \pm 1$ case. The figure indicates that in either the case of $\Delta\mu = 0$ or $\Delta\mu = \pm 1$ the marks ride on the edge of band distribution i.e. near-zig-zag type SWNTs which is consistent with the experimental results presented by Doorn et al.[7] who measured Raman scattering from micelle-dispersed HiPco SWNTs and observed that the near-zig-zag type tubes have stronger scattering intensity than the near-armchair tubes. The same author also showed that the scattering intensity from mod(n - m, 3) = 2 tubes in E^S_{22} transition is one

order higher than that from mod(n - m) = 1 tubes in the same transition, which is agreed by theoretically prediction presented by Grüneis et al.[12] that the optical absorption matrix element is higher for along K-M line than for K-Γ. Therefore, strong scattering would come from near-zig-zag type SWNTs for transitions e.g. E^S_{11}, E^S_{35} for mod(n - m, 3) = 1 tubes, and E^S_{22}, E^S_{24} for mod(n - m, 3) = 2 tubes. When based on the tight-binding and GW-based Kataura plots in Fig. 9, intensely observed $\Delta\mu = \pm 1$ peaks at 145 cm^{-1} for 2.54 eV and 136 cm^{-1} for 2.41 eV would belong either to "E^M_{12} (E^M_{21})" or "E^S_{35} (E^S_{53})", and the peaks at 180 cm^{-1} for 2.54 eV and 166 cm^{-1} for 2.41 eV belong to "E^M_{12} (E^M_{21})".

IV. CONCLUSION

We have investigated resonant Raman scattering from a vertically aligned SWNT film by changing the polarization of the incident laser light with respect to the direction of alignment. It was observed that the shape of the RBM exhibited strong dependence on the polarization. The RBM peaks were grouped into two types according to their behavior: for one type the peak intensity was strong only for perpendicular polarization ($\boldsymbol{e} \perp \boldsymbol{l}$), while the other peaks in parallel polarization ($\boldsymbol{e} \,//\, \boldsymbol{l}$). From the molecular adsorption experiment and the subsequent change in Raman scattering and optical absorption spectra it was evidenced

that the former group originates from $\Delta\mu = \pm 1$ transition while the latter corresponds to $\Delta\mu = 0$ transition. This difference in the nature of RBM peaks relates to the dependence of RBM shapes on the input laser intensity as well as the intensity dependence of frequency, although the observed insensitivity of the intensity of $\boldsymbol{e} \perp \boldsymbol{l}$ peaks toward input laser power requires further investigations. We have unambiguously classified some of RBM peaks into $\Delta\mu = 0$ and $\Delta\mu = \pm 1$ peaks at energies commonly used in RRS (2.41 and 2.54 eV). The knowledge of the nature of each RBM peak elucidated in this report will help provide sounder characterization of SWNT specimens by RRS analysis.

Acknowledgements

The authors express thanks to Profs. M. S. Dresselhaus at MIT and R. Saito at Tohoku Univ. for their valuable discussions, and Mr. T. Sugawara at Univ. of Tokyo for his help in FE-SEM measurements. Part of this work was financially supported by KAKENHI #16360098 and #1610754 from MEXT.

References

1. R. Saito, G. Dresselhaus, and M.S. Dresselhaus, *Physical Properties of Carbon Nanotubes* (Imperial College Press, London, 1998).

2. S. Reich, C. Thomsen, and J. Maultzsch, *Carbon nanotubes* (Wiley-VCH Verlag GmbH & Co. KGaA, Weinheim, 2004).

3. M. S. Dresselhaus and P. C. Eklund, Adv. Phys. **49**, 705 (2000).

4. H. Kuzmany, W. Plank, M. Hulman, Ch. Kramberger, A. Grüneis, Th. Pichler, H. Peterlik, H. Kataura, and Y. Achiba, Eur. Phys. J. B **22**, 307 (2001) 307.

5. A. Jorio, R. Saito, J. H. Hafner, C. M. Lieber, M. Hunter, T. McClure, G. Dresselhaus, and M. S. Dresselhaus, Phys. Rev. Lett. **86**, 1118 (2001).

6. M. S. Strano, S. K. Doorn, E. H. Haroz, C. Kittel, R. H. Hauge, and R. E. Smalley, Nano Lett. **3**, 1091 (2003).

7. S. K. Doorn, D. A. Heller, P. W. Barone, M. L. Usrey, and M. S. Strano, Appl. Phys. A **78**, 1147 (2004).

8. A. Jorio, M. A. Pimenta, A. G. Souza Filho, Ge. G. Samsonidze, A. K. Swan, M. S. Ünlü, B. B. Goldberg, R. Saito, G. Dresselhaus, and M. S. Dresselhaus, Phys. Rev. Lett. **90**, 107403 (2003).

9. H. Kataura, Y. Kumazawa, Y. Maniwa, I. Umezu, S. Suzuki, Y. Ohtsuka, and Y. Achiba, Synth. Met. **103**, 2555 (1999).

10. H. Ajiki and T. Ando, Physica B **201**, 349 (1994).

11. I. Božović, N. Božović, and M. Damnjanovic, Phys. Rev. B **62**, 6971 (2000).

12. A. Grüneis, R. Saito, Ge. G. Samsonidze, T. Kimura, M. A. Pimenta, A. Jorio, A. G. Souza Filho, G. Dresselhaus, and M. S. Dresselhaus, Phys. Rev. B **67**, 165402 (2003).

13. A. Jorio, G. Dresselhaus, M. S. Dresselhaus, M. Souza, M. S. S. Dantas, M. A. Pimenta, A. M. Rao, R. Saito, C. Liu, and H. M. Cheng, Phys. Rev. B **85**, 2617 (2000).

14. J. Hwang, H. H. Gommans, A. Ugawa, H. Tashiro, R. Haggenmueller, K. I. Winey, J. E. Fischer, D. B. Tanner, and A. G. Rinzler, Phys. Rev. B **62**, R13310 (2000).

15. G. S. Duesberg, I. Loa, M. Burghard, K. Syassen, and S. Roth, Phys. Rev. Lett. **85**, 5436 (2000).

16. A. Jorio, A. G. Souza Filho, V. W. Brar, A. K. Swan, M. S. Ünlü, B. B. Goldberg, A. Righi, J. H. Hafner, C. M. Lieber, R. Saito, G. Dresselhaus, and M. S. Dresselhaus, Phys. Rev. B **65**, 121402 (2002).

17. A. Grüneis, R. Saito, J. Jiang, Ge. G. Samsonidze, M. A. Pimenta, A. Jorio, A. G. Souza Filho, G. Dresselhaus, and M. S. Dresselhaus, Chem. Phys. Lett. **387**, 301 (2004).

18. R. B. Weisman and S. M. Bachilo, Nano Lett. **3** (2003) 1235.

19. Y. Murakami, S. Chiashi, Y. Miyauchi, M. Hu, M. Ogura, T. Okubo, and S. Maruyama, Chem. Phys. Lett. **385**, 298 (2004).

20. S. Maruyama, R. Kojima, Y. Miyauchi, S. Chiashi, and M. Kohno, Chem. Phys. Lett. **360**, 229 (2002).

21. Y. Murakami, Y. Miyauchi, S. Chiashi, and S. Maruyama, Chem. Phys. Lett. **374**, 53 (2003).

22. S. Maruyama, E. Einarsson, Y. Murakami, and T. Edamura, Chem. Phys. Lett. (Submitted).

23. A. Jorio, M. A. Pimenta, A. G. Souza Filho, R. Saito, G. Dresselhaus, and M. S. Dresselhaus, New J. Phys. **5**, 139 (2003).

24. H. D. Li, K. T. Yue, Z. L. Lian, Y. Zhan, L. X. Zhou, S. L. Zhang, Z. J. Shi, Z. N. Gu, B. B. Liu, R. S. Yang, H. B. Yang, G. T. Zou, Y. Zhang, and S. Iijima, Appl. Phys. Lett. **76**, 2053 (2000).

25. N. R. Raravikar, P. Keblinski, A. M. Rao, M. S. Dresselhaus, L. S. Schadler, and P. M. Ajayan, Phys. Rev. B **66**, 235424 (2002).

26. S. Chiashi, Y. Murakami, Y. Miyauchi, and S. Maruyama, Chem. Phys. Lett. **386**, 89 (2004).

27. Y. Murakami, E. Einarsson, and S. Maruyama, Carbon. (To be submitted).

28. A. Kukovecz, Ch. Kramberger, V. Georgakilas, M. Prato, and H. Kuzmany, Euro. Phys. J. B **28**, 223 (2002).

29. Y. Miyauchi, S. Chiashi, Y. Murakami, Y. Hayashida, and S. Maruyama, Chem. Phys. Lett. **387**, 198 (2004).

30. J. Kürti, G. Kresse, and H. Kuzmany, Phys. Rev. B **58**, R8869 (1999).

31. D. Sánchez-Portal, E. Artacho, J. M. Soler, A. Rubio, and P. Ordejón, Phys. Rev. B **59**, 12678 (1999).

32. S. M. Bachilo, M. S. Strano, C. Kittrell, R. H. Hauge, R. E. Smalley, R. B. Weisman, Science **298**, 2361 (2002).

33. M. S. Strano, J. Am. Chem. Soc. **125**, 16148 (2003).

34. S. D. M. Brown, A. Jorio, P. Corio, M. S. Dresselhaus, G. Dresselhaus, R. Saito, and K. Kneipp, Phys. Rev. B **63**, 155414 (2001).

35. M. S. Strano, C. A. Dyke, M. L. Usrey, P. W. Barone, M. J. Allen, H. Shan, C. Kittrell, R. H. Hauge, J. M. Tour, and R. E. Smalley, Science **301**, 1519 (2003).

36. M. S. Strano, C. B. Huffman, V. C. Moore, M. J. O'Connell, E. H. Haroz, J. Hubbard, M. Miller, K. Rialon, C. Kittrell, S. Ramesh, R. H. Hauge, and R. E. Smalley, J. Phys. Chem. B **107**, 6979 (2003).

37. S. Maruyama, T. Miyake, S. Okada, S. Ogawa, and K. Oba, Chem. Phys. Lett. (To be submitted).

38. R. Saito, G. Dresselhaus, and M. S. Dresselhaus, Phys. Rev. B **61**, 2981 (2000).

Figure captions

FIG. 1. A cross-sectional FE-SEM image of a vertically aligned SWNT film at a fractured edge of the quartz substrate taken from tilted angle (top) and horizon (bottom)

FIG. 2. Schematical description of relationships between the laser propagation direction (***k***), the laser polarization direction (***e***), and the SWNT axis direction (***l***) in the measurement.

FIG. 3. RBM spectra measured by 488, 514.5, and 633 nm lasers for different incident configurations (i - iv, see text). G band spectra taken at 488 nm are also shown. The RBM spectra were normalized by the corresponding G^+ height and decomposed into Lorentzian curves by maintaining the FWHM values within a spectrum. Asterisks denote the peaks dominantly observed in parallel polarization condition. The oscillatory line on the baseline denotes differential between experimental spectrum and sum of Lorentzian curves.

FIG. 4. RBM spectra taken at 488 nm with laser light incident (a) from side and (b) from top of the film. A polarizer was inserted in a scattering light path except the case denoted "-All". The "X-Y" description represents the polarization directions of incident and scattered light.

FIG. 5. The change in intensities of selected RBM peaks divided by the G^+ band among "from top" - "45°" - "parallel" conditions for (a) 488 and (b) 514.5 nm. The ordinate was normalized by the values of the "from top" condition.

FIG. 6. The change in RBM spectra measured in the "from top" condition by 488 nm light. The spectra are (a) the as-synthesized sample and (b) after evacuation by an oil-pump for 1h at

200°C. The original spectrum of a different molecule-adsorbed sample (c) is recovered after heating it at 200°C for 1 h in a CVD chamber evacuated by an oil-free pump (d). The spectra are normalized by the height of the G^+ peak. The right panel shows corresponding tangential mode spectra of (a) and (b).

FIG. 7. Optical absorption spectra of (b) an adsorbed sample and (c) the same sample after recovery by heating in vacuum at 200°C for 1 h. In the inset are corresponding Raman spectra taken at 488 nm in the "from top" configuration, along with (a) the original spectra before adsorption, to which all spectra are normalized by the height of the G^+ band. Asterisks indicate the switching noise of the spectrophotometer.

FIG. 8. (a) Spectral change of RBM peaks by changing the laser power intensity from 0.75 to 2.42 mW, using 488 nm light in the "from top" configuration. The spectra were normalized by the G^+ band. (b) The intensity variance of each Lorentzian-decomposed RBM peak over the incident laser power. Ordinate values were normalized by those in the case of 0.75 mW. (c) The relationship between the frequency downshift of RBM peak and that of the G^+ peak by heating of SWNTs, both from the case of 0.75 mW.

FIG. 9. The locations of several unambiguous $\boldsymbol{e} \,//\, \boldsymbol{l}$ ($\Delta\mu = 0$) peaks marked with circles and $\boldsymbol{e} \perp \boldsymbol{l}$ ($\Delta\mu = \pm 1$) with crosses on a Kataura plot calculated from tight-binding (solid symbols) and GW-method (open symbols). Panels in the upper row represent the plots for the $\Delta\mu = 0$ transition while panels in the lower row correspond $\Delta\mu = \pm 1$.

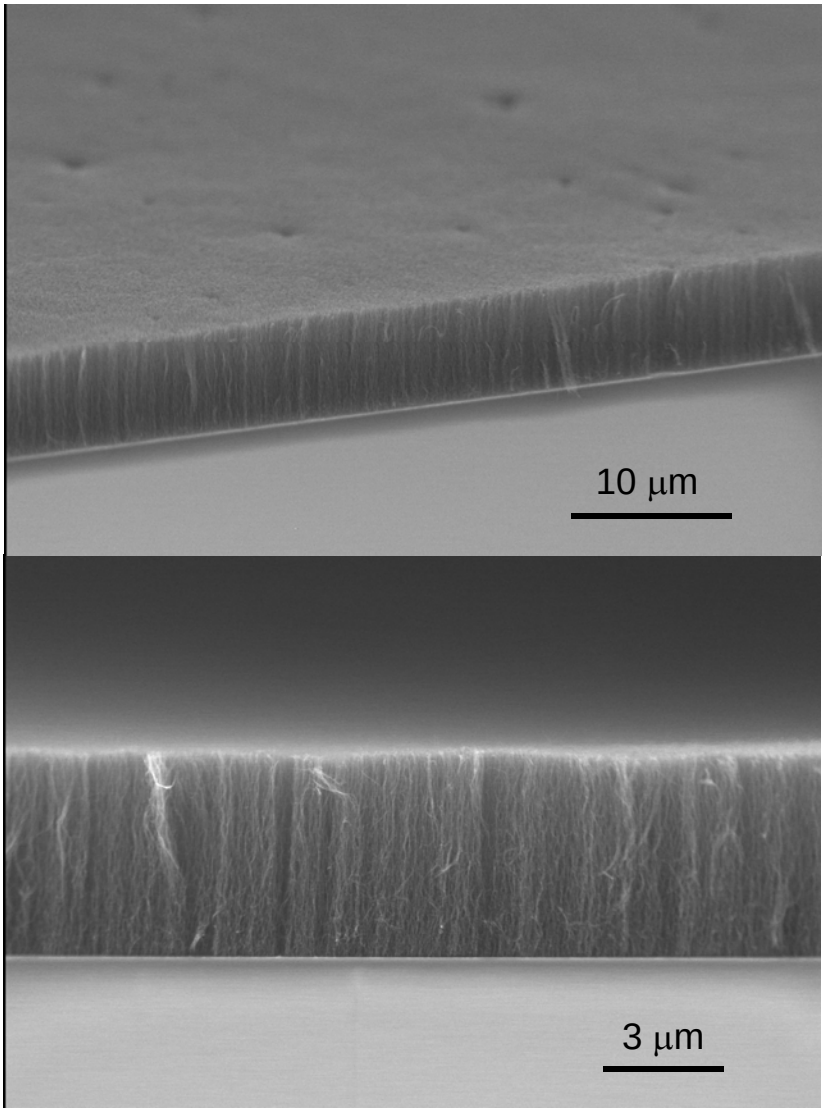

Figure 1

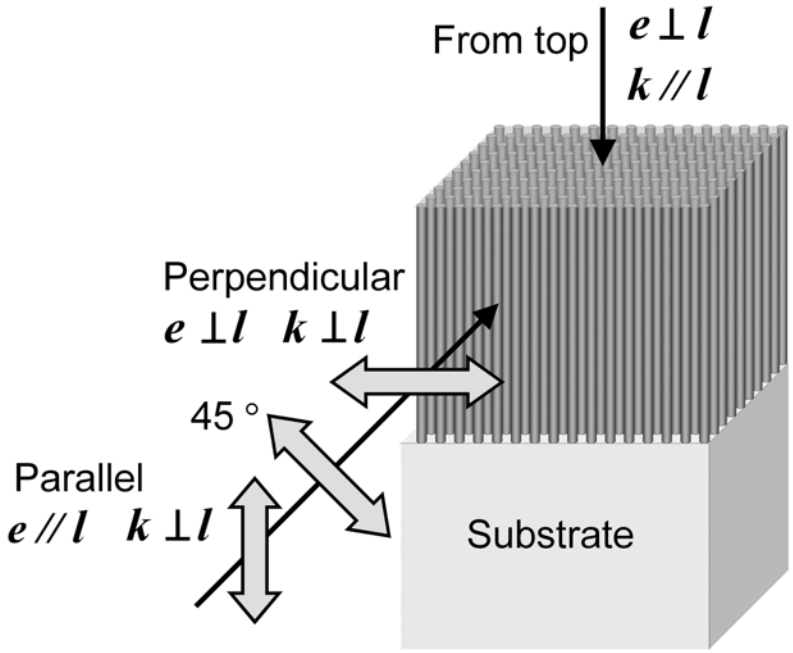
From top
e ⊥ l
k // l
Perpendicular
e ⊥ l k ⊥ l
45 °
Parallel
e // l k ⊥ l
Substrate

Figure 2

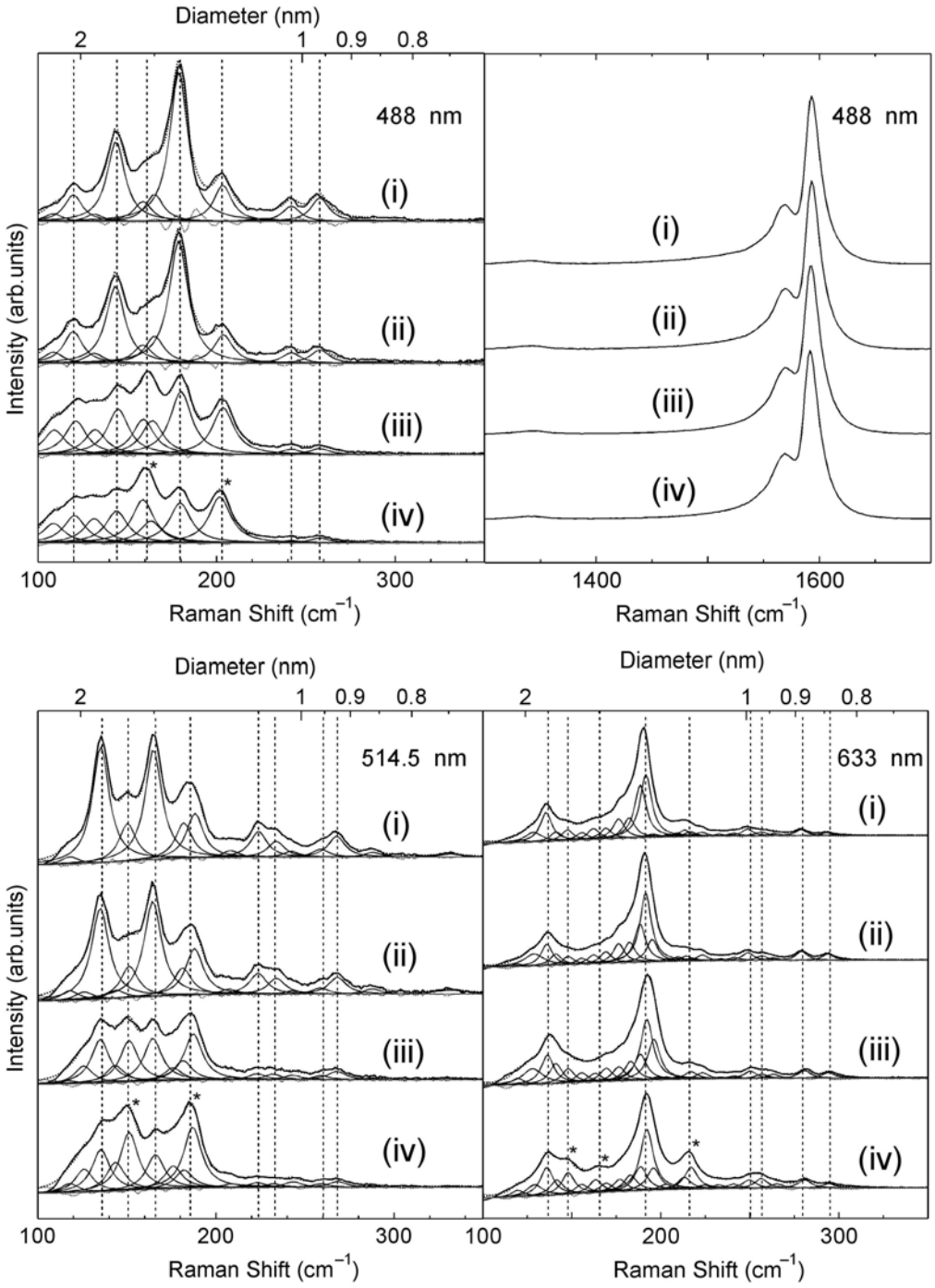
Diameter (nm)
2
1
0.9
0.8
488 nm
(i)
(ii)
(iii)
(iv)
Intensity (arb.units)
100
200
300
Raman Shift (cm^{-1})
1400
1600
514.5 nm
633 nm
*

Figure 3

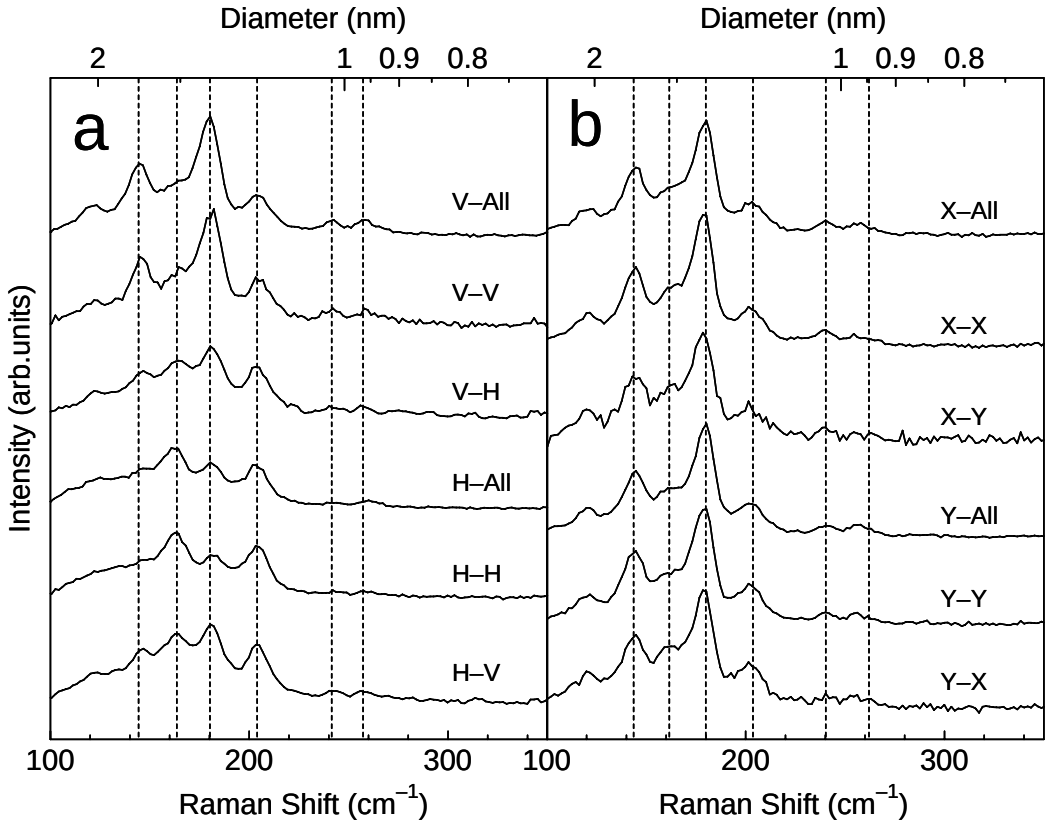
Diameter (nm)
2
1
0.9
0.8
a
b
V–All
V–V
V–H
H–All
H–H
H–V
X–All
X–X
X–Y
Y–All
Y–Y
Y–X
Intensity (arb.units)
100
200
300
Raman Shift (cm^{-1})

Figure 4

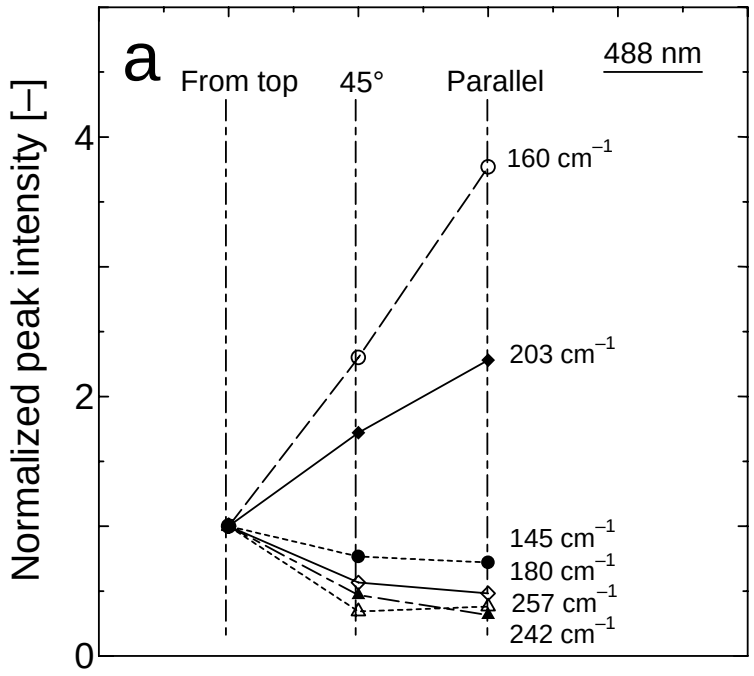
a
From top
45°
Parallel
488 nm
Normalized peak intensity [–]
0
2
4
160 cm–1
203 cm–1
145 cm–1
180 cm–1
257 cm–1
242 cm–1

Figure 5(a)

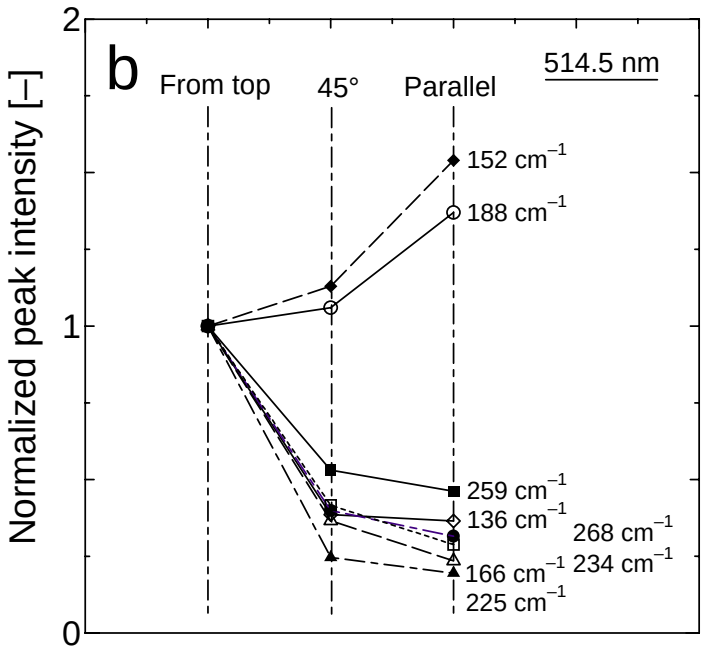
b
From top
45°
Parallel
514.5 nm
Normalized peak intensity [–]
2
1
0
152 cm–1
188 cm–1
259 cm–1
136 cm–1
268 cm–1
166 cm–1
234 cm–1
225 cm–1

Figure 5(b)

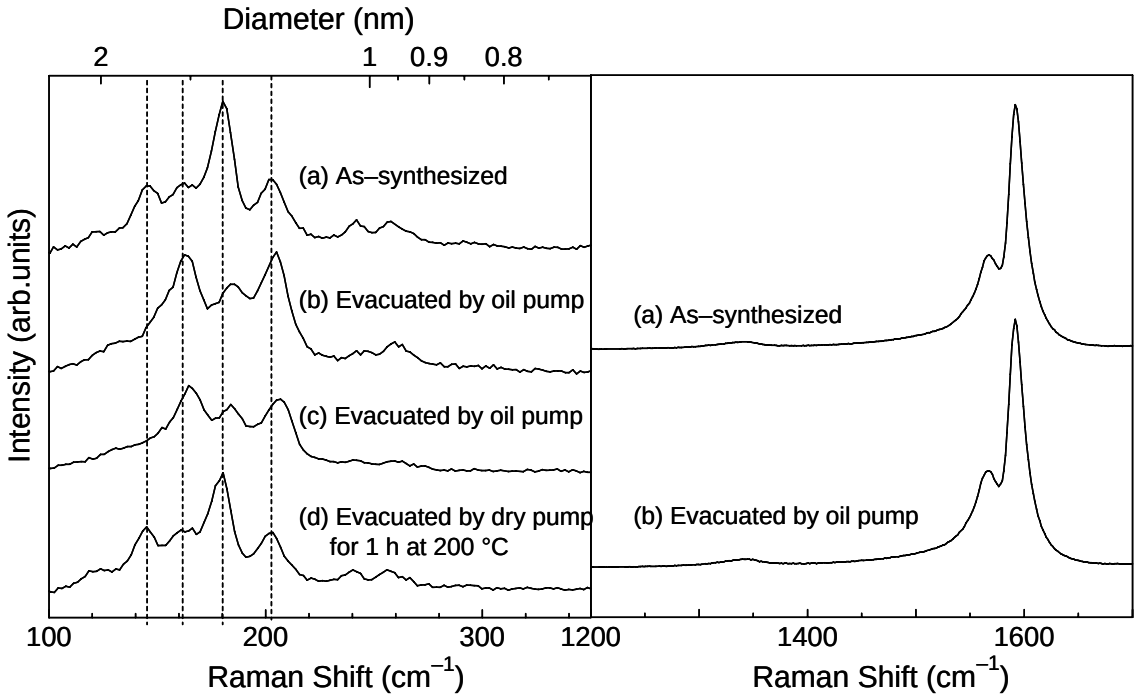
Diameter (nm)
2
1
0.9
0.8
Intensity (arb.units)
(a) As–synthesized
(b) Evacuated by oil pump
(c) Evacuated by oil pump
(d) Evacuated by dry pump
for 1 h at 200 °C
100
200
300
Raman Shift (cm^{-1})
1200
1400
1600
Raman Shift (cm^{-1})
(a) As–synthesized
(b) Evacuated by oil pump

Figure 6

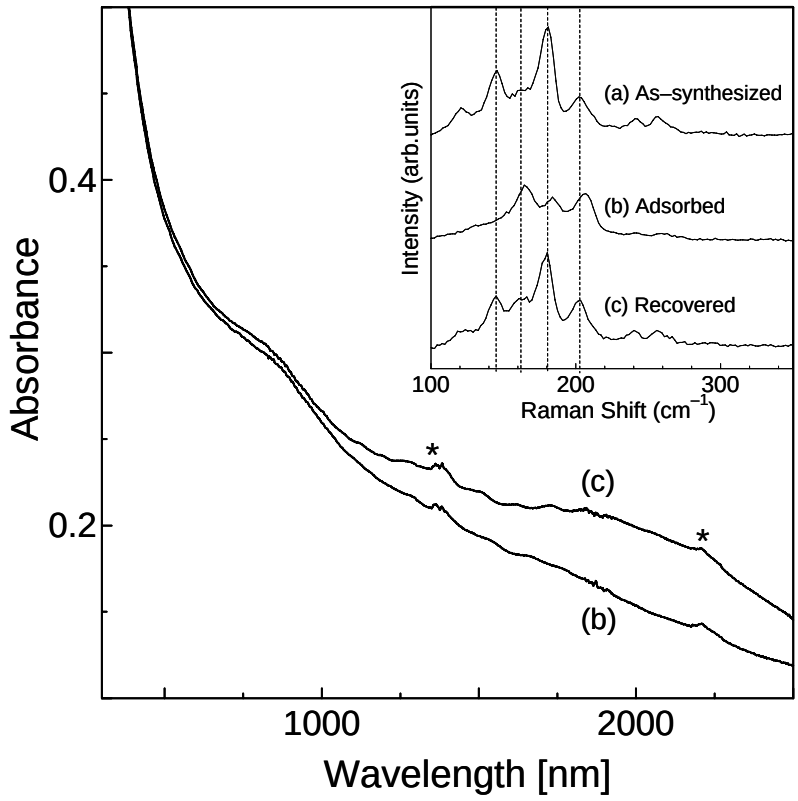
Absorbance
0.4
0.2
1000
2000
Wavelength [nm]
(c)
(b)
*
*
Intensity (arb.units)
(a) As–synthesized
(b) Adsorbed
(c) Recovered
100
200
300
Raman Shift (cm^{-1})

Figure 7

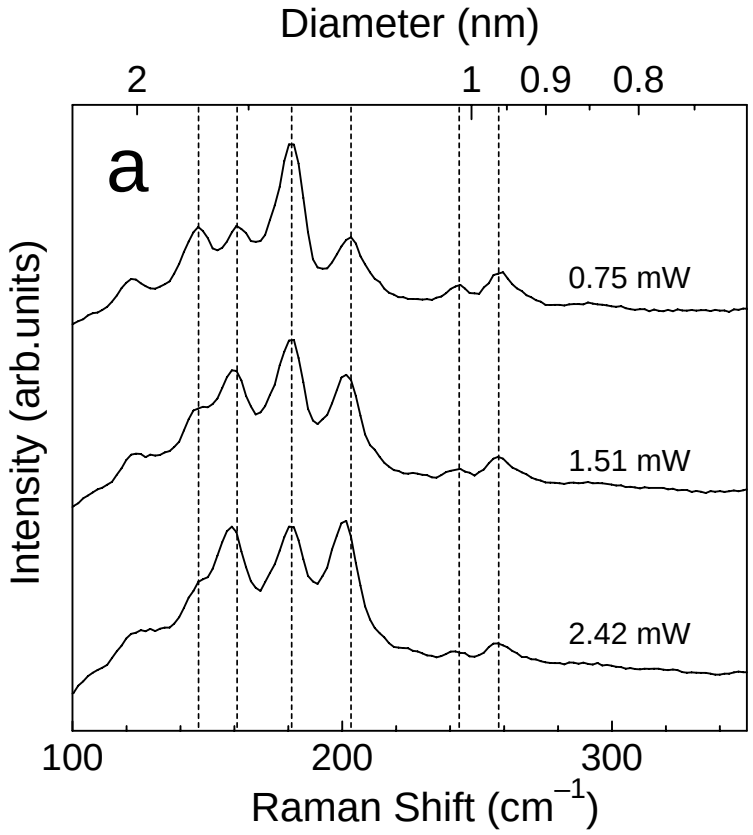
Diameter (nm)
2
1
0.9
0.8
a
0.75 mW
1.51 mW
2.42 mW
Intensity (arb.units)
100
200
300
Raman Shift (cm^{-1})

Figure 8(a)

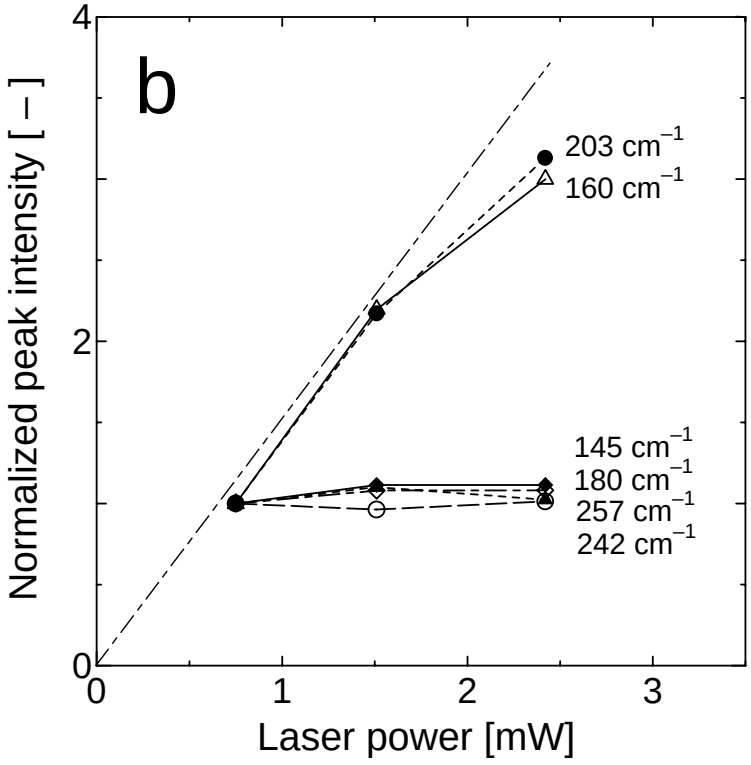
b
Normalized peak intensity [–]
Laser power [mW]
0
1
2
3
4
203 cm−1
160 cm−1
145 cm−1
180 cm−1
257 cm−1
242 cm−1

Figure 8(b)

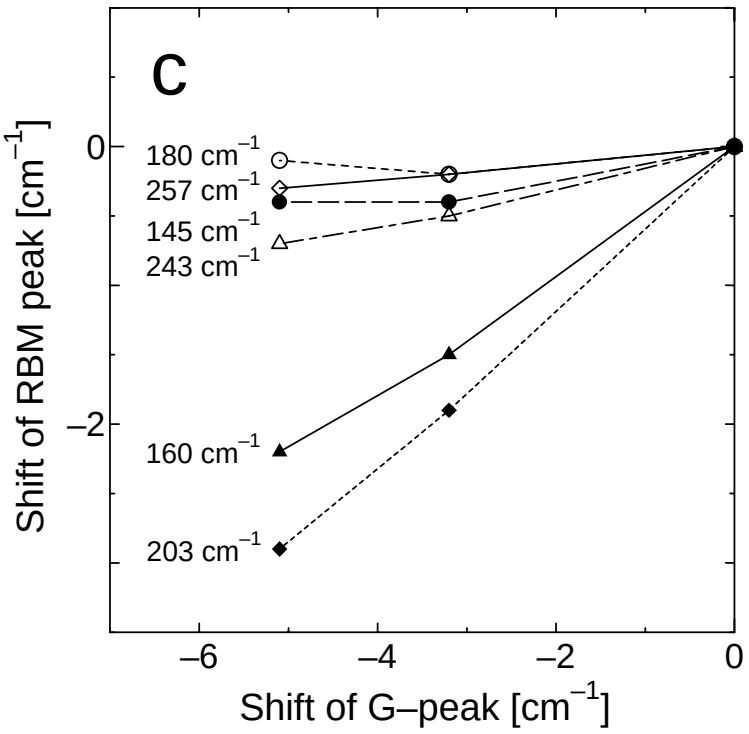
C
0
–2
180 cm–1
257 cm–1
145 cm–1
243 cm–1
160 cm–1
203 cm–1
–6
–4
–2
0
Shift of RBM peak [cm–1]
Shift of G–peak [cm–1]

Figure 8(c)

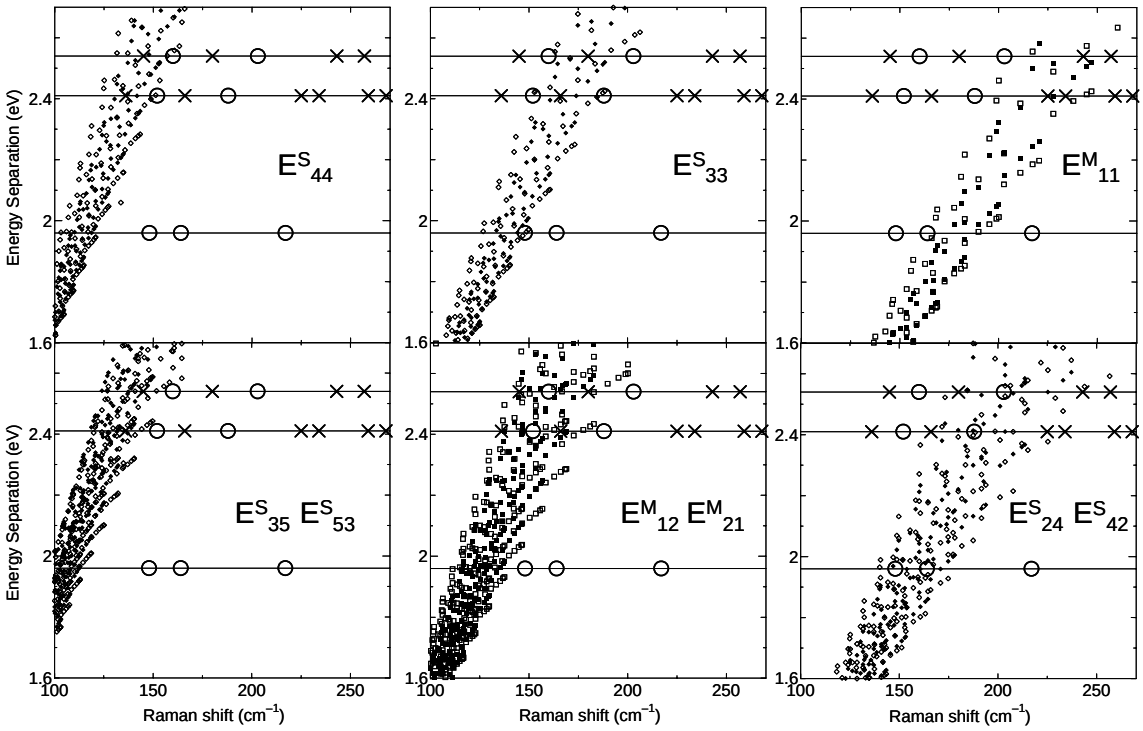
Energy Separation (eV)
Raman shift (cm^{-1})
E^S_{44}
E^S_{33}
E^M_{11}
E^S_{35} E^S_{53}
E^M_{12} E^M_{21}
E^S_{24} E^S_{42}

Figure 9